Investigation of InN layers grown by molecular beam epitaxy on GaN templates

A. Vilalta-Clemente*,1, G. R. Mutta1, M. P. Chauvat1, M. Morales1, J. L. Doualan1, P. Ruterana1, J. Grandal2, M. A. Sánchez-García2, F. Calle2, E. Valcheva3, and K. Kirilov3

1 CIMAP UMR 6252 CNRS-ENSICAEN-CEA-UCBN, 6, Boulevard du Maréchal Juin, 14050 Caen Cedex, France
2 ISOM and Department de Ingeniería Electrónica, E.T.S.I. Telecomunicación, Universidad Politécnica de Madrid, Ciudad Universitaria, 28040 Madrid, Spain
3 Faculty of Physics, Sofia University, 5J. Boucher Blvd., 1164 Sofia, Bulgaria

* Corresponding author: e-mail arantxa.vilalta-clemente@ensicaen.fr, Phone: +33 231 452 663, Fax: +33 231 452 557

An investigation of InN layers grown on GaN templates by molecular beam epitaxy (MBE) has been carried out by X-ray diffraction (XRD), Raman spectroscopy (RS) and photo-luminescence (PL). A good correlation is noticed between their crystalline quality and optical properties. The best samples exhibit a PL emission between 0.6 and 0.7 eV. The surface structure was quite different from one sample to the other, pointing out to a critical role of the growth conditions, which probably need to be tightly optimized for a good reproducibility.

1 Introduction InN is still an emerging material of the nitride semiconductors family, which has many interesting properties, such as a high theoretical mobility for electron of $4400\,cm^2\,V^{-1}\,S^{-1}$ at 300 K and of course its small band gap<0.7 eV [1]. In the last few years it has been the topic of extensive research as a promising material for many applications [1, 2]. Obviously, such properties should be at the origin of devices compatible with the wavelengths of the optical fibres in optical telecommunication systems, for instance laser diodes and also those in high frequency electronics devices [3, 4]. Moreover, it may also play a crucial role in the fabrication of highest efficiency InN photovoltaic devices [5, 6], by band gap engineering from below 0.7 eV (InN) to 6.2 eV (AlN) through 3.4 eV (GaN). Of course, in this instance, important problems for the epitaxial growth of high mismatch materials need to be solved. Furthermore, InGaN alloys are presumed to exhibit superior resistance against radiation damages in comparison to others solar cells materials (GaAs and InGaP) [5].

Currently, InN thin films of good crystalline quality can be obtained by molecular beam epitaxy (MBE) and metalorganic vapour phase epitaxy (MOVPE). In the following, we present the results obtained on the structural properties of MBE InN layer grown of (0001) sapphire. We have analysed the residual strain by X-ray diffraction (XRD)

and Raman spectroscopy (RS). The results will be discussed in the light of the optical properties as measured by photoluminescence (PL) and absorption.

2 Experimental The investigated (0001) InN layers were grown by plasma enhanced MBE at 450 °C, on sapphire substrates on top of which there was a 5 μm GaN hydride vapour epitaxial template and another MBE buffer layer (150 nm) deposited at 730 °C. The studied five specimens (samples A–E) exhibited nominal thicknesses in the 150–750 nm range. All the samples were grown in indium-rich conditions except sample C. The films were characterized by atomic force microscopy (AFM) using a Digital Instruments Nanoscope III, operated in tapping mode. Areas of $1\,\mu m \times 1\,\mu m$ were scanned in different places to ensure that AFM images are representative of the film surface. The in-plane residual strain of these films was investigated by high-resolution X-ray diffraction (HRXRD) and RS measurements. The diffraction studies were performed using a Philips X'Pert MRD triple axis diffractometer equipped with a four-bounce (220)-Ge monochromator and operating at the Cu $K_{\alpha1}$ radiation ($\lambda_{CuK\alpha1} = 1.54056$ Å). The InN and GaN c-lattice parameters were obtained from the position of the symmetric (0002) and (0004) reflections in order to estimate the normal ε_{zz} strain for both phases in the epitaxial

layers. We systematically performed also ω-scans (rocking curve) of the symmetric (0002) reflection of InN in order to access the crystalline mosaicity of the thin films ($\Delta\omega_c$).

Micro-Raman measurements were performed with a LabRam HR spectrometer in backscattering geometry and using a 632 nm excitation laser with a spot size of about 1 µm. The spectral resolution was $1\,\mathrm{cm}^{-1}$. This geometry allowed the measurement of the E_2 phonon mode peak position, for which the shift is correlated with the stress induced in the InN layers during the growth. However, as the reported stress-free Raman frequencies for InN are still scattered in quite extended range (483–$495\,\mathrm{cm}^{-1}$), our aim will be to extract the main trends on the evolution of strain in these samples.

The above samples were also investigated by PL using an argon laser, we shall discuss the results obtained at room temperature. The detection system is constituted by an InGaAs detector in the infrared and we switch to a photo-multiplier around 1 µm wavelength. The measurements took place in one run for an easier comparison of the samples.

3 Results

3.1 The surface morphology
From the AFM analysis of the samples as shown in Fig. 1, it can be noticed that at this scale, we have important change in the surface state from one sample to the next. However, no microcracks have been observed in any of the investigated samples, in contrast a report by other authors who used a similar growth technique [7]. Apart from one of the two samples with 250 nm thickness (C), the RMS roughness exhibited by all the others is smaller than 0.8 nm showing that quite smooth films have been obtained. Moreover, the surface morphology of sample A, D and E is suggestive of step-flow growth and in the samples A and E atomic terraces are clearly visible,
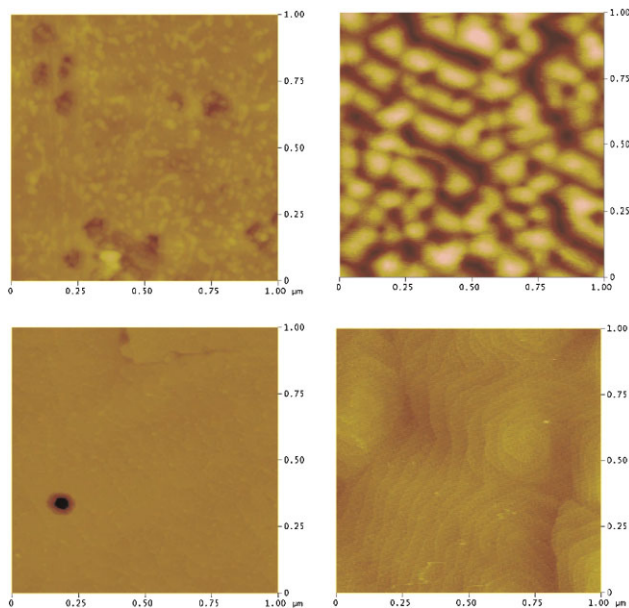
which is a proof that in these instances, the dominant growth mode has been two-dimensional (2D). For sample C, we point out more or less elongated and irregular shape islands which may indicate some columnar growth (pronounced 3D mode). In this case, we measure the highest roughness above 7 nm, with a z-scale of 40 nm (Table 2). From these observations, it can be noticed that the InN layer thickness may not be the most critical parameter for the surface layer morphology. For instance, the difference between the surface structure of samples B and C (250 nm) is due to change in growth parameters, which in sample C, resulted in a pronounced 3D growth mode (higher temperature and nitrogen rich conditions). Interestingly, as mentioned above, the surfaces of samples A (not shown) and E exhibit clear atomic steps, which is an indication that the growth mode may not necessarily change with the deposited thickness.

3.2 The residual stress
In the analysis of the HRXRD measurements, the normal ε_{zz} strain tensor components have been obtained from $\varepsilon_{zz} = (c-c_0)/c_0$, where c and c_0 are the strained and unstrained lattice parameters. The reference values of the bulk lattice parameters of strain-free InN and GaN were taken $c_{0\,\mathrm{InN}} = 5.669$ Å (JCPDS 88-2362) and $c_{0\,\mathrm{GaN}} = 5.142$ Å (JCPDS 88-2361), respectively [8]. The corresponding stress tensor follows Hooke's law as:

$$\sigma_{xx} = (C_{11} + C_{12})\varepsilon_{xx} + C_{13}\varepsilon_{zz},$$
$$\sigma_{zz} = 2C_{13}\varepsilon_{xx} + C_{33}\varepsilon_{zz}.$$

Under (0001) biaxial strain, as $\sigma_{zz} = 0$, ε_{zz} and the in-plane ε_{xx} and ε_{yy} strain tensor components are correlated by: $\varepsilon_{xx} = \varepsilon_{yy} = -(C_{33}/2C_{13})\varepsilon_{zz}$ and the in-plane strain is estimated from the HRXRD deduced ε_{zz}. Subsequently, the in-plane residual stress σ_{xx} for both InN and GaN are calculated from: $\sigma_{xx} = (-C_{33}/(2C_{13})(C_{11}+C_{12}) + C_{13})\varepsilon_{zz}$.

In this work, we used two different C_{ij} stiffness coefficients sets, as reported respectively by Wright [9] and Kim et al. [10] (Table 1).

For all the samples and independent of the chosen reference for the stiffness coefficients, the negative values of σ_{xx} indicate that InN (Table 2) and GaN films exhibit compressive in-plane biaxial stress. This is in agreement with the results reported by Trybus et al. who have also investigated MBE GaN thin films [6]. There appears to be a quite general trend in these films, above 250 nm thickness, the stress remains almost constant at around -2.5 GPa. For the GaN layer, σ_{xx} is in the -6.8 to -9.1 GPa range (not

Figure 1 (online colour at: www.pss-a.com) AFM images of samples B-C (top) and D-E (bottom).

Table 1 Theoretical C_{ij} stiffness coefficients of InN.

elastic constants	Kim et al. [10]	Wright [9]
C_{11} (GPa)	271	223
C_{12} (GPa)	124	115
C_{13} (GPa)	94	92
C_{33} (GPa)	200	224
C_{44} (GPa)	46	48

Original
Paper

Phys. Status Solidi A **207**, No. 5 (2010)

1081

Table 2 Structural parameters as deduced from HRXRD and AFM surface roughness for the five studied InN films.

| sample		A	B	C	D	E
thickness (nm)		150 nm	250 nm	250 nm	400 nm	750 nm
growth temperature (°C)		475	400	490	455	450
c (Å)	HRXRD	5.727	5.710	5.711	5.717	5.708
a (Å)	Kim et al.	3.463	3.474	3.471	3.469	3.475
	Wright	3.457	3.470	3.469	3.465	3.472
σ_{xx} (GPa)	Kim et al.	−3.338	−2.359	−2.665	−2.762	−2.244
	Wright	−3.269	−2.311	−2.367	−2.705	−2.198
$FWHM_{002}$ (°)		0.0760	0.3328	0.2913	0.1871	0.2128
$\Delta\omega_c$ (°)		0.1502	0.2223	0.1719	0.1393	0.1357
RMS (nm)		0.714	1.430	7.556	0.785	0.393

presented here) showing that the lattice mismatch between the layer and the substrate is probably taking part in the measured residual stresses. Indeed the lattice mismatch between the sapphire and GaN is 16% whereas the one between InN and GaN is 11%. Using the C_{ij} of Wright or Kim et al., we obtained very close σ_{xx} values for each sample (Fig. 2, top). For sample B and C exhibiting the same thickness with the C_{ij} values reported by Kim et al. we have a σ_{xx} difference of −0.31 GPa between the two samples, whereas with Wright C_{ij} set we obtained only a difference of −0.05 GPa. This may be indicative of a different strain relaxation mechanism in the two layers.

For the calculation of the stress, many authors have used the InN unstrained $c_{0\ InN}$ (5.7033 Å) of Paszkowicz et al. [11]. With such a parameter, independent of the C_{ij} set of coefficients [9, 10], the σ_{xx} is shifted by ∼2 GPa (not shown here). In fact, the reported lattice parameters are rather scattered: 5.54–5.8002 Å for $c_{0\ InN}$ and 3.483–3.5848 Å for $a_{0\ InN}$ parameters [12]. Therefore, in order to have the most appropriate unstrained c-parameter, it would be interesting to have test samples with 10 or 20 μm InN thickness in which the strain is released close to a powder.

As the same trend for scattered values was observed for the reported C_{ij} in the literature, the determination of the ratio

$C_{33}/2C_{13}$ is of prior importance. To this end, the measurement of the a-parameter of the InN films is in progress through the measurement of the asymmetric $(10\bar{1}\ell)$ reflections. The evolution of the σ_{xx} in-plane residual stress obtained by HRXRD was compared to that given by the E_2 high mode frequency position shift as shown in Fig. 2 (lower curve). The E_2 shift evolution (Fig. 2 right vertical scale) versus the layer thickness exhibits a similar behaviour as the σ_{xx}. Moreover, when we use a strain-free Raman frequency InN E_2 mode of 491.4 cm^{-1} as determined recently by Darakchieva et al. [13], we observe compressive in-plane residual stress for all the samples in agreement with our HRXRD studies.

3.3 The InN layers mosaicity The smallest full-width at half-maximum of the InN (0002) reflection peak ($FWHM_{0002}$) was observed from sample A (0.076°), this is quite close to that reported for the same InN films deposited by MOVPE [14]. This sample exhibits also a mosaicity $\Delta\omega_c$, extracted from the (0002) ω-scan, of around 0.15° which indicates that the crystalline quality along the c-axis was the highest among the five samples. However, it also exhibits the larger compressive in-plane residual stress (Table 2). The mosaicity $\Delta\omega_c$ increases when the InN thickness goes from 150 to 250 nm. This suggests that the films consist in small crystalline domains, whose c-axis are tilted from one another; the 100 nm thickness increase leads to larger domains with higher tilts. In agreement with the behaviour of InN layers deposited on GaN substrates by MOVPE [15], the measured mosaicity then decreases with increasing thickness and saturates at around 0.136° for the sample E (750 nm). If we consider that the reduction of $\Delta\omega_c$ starts to indicate coalescence (initiating a 2D growth mode), this process seems to be disrupted between 150 and 400 nm layer thickness. As can be noticed, we have a small $\Delta\omega_c$ in sample A, and a substantial increase for sample B and C which in addition exhibit quite different morphology. Then from samples C to E this parameter undergoes a slow decrease and a substantial 2D growth mode with surface steps and minimum roughness only becomes dominant in sample E. This behaviour seems to point to complex strain relaxation mechanisms, which need more work to understand.
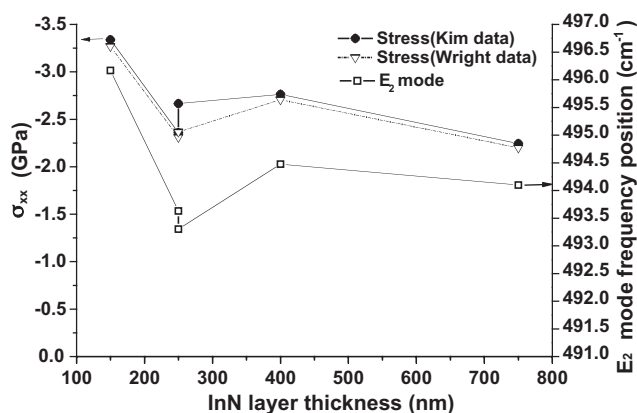
Figure 2 In-plane residual stress σ_{xx} as deduced from HRXRD and E_2 high mode frequency position evolution with the InN layer thickness.
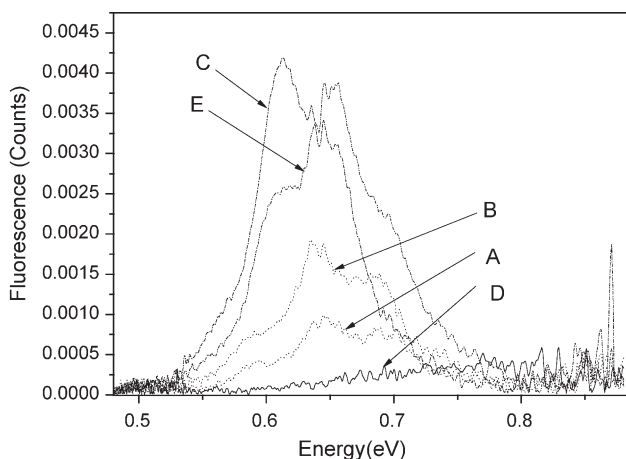
Figure 3 PL of the InN layers.

3.4 Optical properties From the PL data (Fig. 3), as can be noticed, there is an important variation in the emission intensity from one sample to the next. However except for sample D (low signal), the peak positions can be clearly identified and they are located between 0.6 and 0.7 eV, which is consistent with the results published for good quality InN layers [1, 16–18]. We also have attempted to determine the band gap by measuring the absorption. Unfortunately, in none of the samples, it has been possible to measure the transmitted signal. The absence of such signal is not understood at the time being and our next step is to carry out TEM measurements in order to look for any structural or chemical origin of this behaviour.

4 Discussion and conclusions From the above results, it is pointed out that the stress tends to decrease at large layer thickness. However, we interestingly notice that the layers with 150 nm thickness exhibit surface atomic steps (2D step flow growth mode) and low mosaicity. The best crystalline quality at this thickness comes along with a large surface roughness (0.714 nm) and compressive biaxial stress (3.3 GPa), this is lost for B–D samples of intermediate thicknesses. Therefore, the large strain at the InN/GaN (11%) is not easy to relax through the formation of misfit dislocations and/or other defects close to the interface and more investigations are necessary in order to determine the operating mechanisms. For the largest sample thickness (E: 750 nm), we seem to approach some stable structure of the film, with step flow, and minimum surface roughness (RMS: 0.39 nm). The intermediate thickness layers present complex features which are not easy to interpret, based only on our present investigation. However, as pointed out above, we notice that at about 250 nm thickness, we have two possible operating mechanisms which disrupted the step flow growth mode seen in the 150 nm sample. (i) In sample C, there is a substantial 3D growth mode with large islands (RMS: 7.5 nm), smaller compressive biaxial stress and slightly

higher tilt than in the sample A. (ii) The more complex structure of sample B, which is also still operating in sample D, but in a lesser degree as the latter exhibits patches of step flow growth areas.

In these layers, a low stress correlates with a high PL intensity. Samples E (750 nm), which exhibits a surface morphology with atomic steps, provided a high PL signal. One point to be noticed is the highest PL emission of sample C, which means that each individual island is of good quality.

References

[1] A. G. Bhuiyan, A. Hashimoto, and A. Yamamoto, J. Appl. Phys. **94**, 2779 (2003).
[2] S. C. Jain, M. Willander, J. Narayan, and R. V. Overstraeten, J. Appl. Phys. **87**, 965 (2000).
[3] J. W. Orton and C. T. Foxon, Rep. Prog. Phys. **61**, 1–75 (1998).
[4] Hai. Lu, William. J. Schaff, and Lester. F. Eastman, J. Appl. Phys. **96**, 3577 (2004).
[5] J. Wu, W. Walukiewicz, K. M. Yu, W. Shan, J. W. Ager, III, E. E. Haller, Hai. Lu, William. J. Schaff, W. K. Metzger, and S. Kurtz, J. Appl. Phys. **94**, 6477 (2003).
[6] E. Trybus, G. Namkoong, W. Henderson, S. Burnham, W. A. Doolittle, M. Cheung, and A. Cartwright, J. Cryst. Growth **288**, 218 (2006).
[7] E. Dimakis, E. Iliopoulos, K. Tsagaraki, A. Adikimenakis, and A. Georgakilas, Appl. Phys. Lett. **88**, 191918 (2006).
[8] A. F. Wright and J. S. Nelson, Phys. Rev. B: Condens. Matter **51**, 7866 (1995).
[9] A. F. Wright, J. Appl. Phys. **82**, 2833 (1997).
[10] K. Kim, W. R. L. Lambrecht, and B. Segall, Phys. Rev. B **53**, 16310 (1996).
[11] W. Paszkowicz, Powder Diffr. **14**, 258 (1999).
[12] W. Paszkowicz, R. Cerny, and S. Krukowski, Powder Diffr. **18**, 114 (2003).
[13] V. Darakchieva, P. P. Paskov, E. Valcheva, T. Paskova, B. Monemar, M. Schubert, H. Lu, and W. J. Schaff, Appl. Phys. Lett. **84**, 3636 (2004).
[14] C. Yang, X. Wang, H. Xiao, X. Zhang, G. Hu, J. Ran, C. Wang, J. Li, J. Li, and Z. Wang, Appl. Surf. Sci. **255**, 3149 (2008).
[15] S. Yamaguchi, M. Kariya, S. Nitta, T. Takeuchi, C. Wetzel, H. Amano, and I. Akasaki, J. Appl. Phys. **85**, 7682 (1999).
[16] P. Singh, P. Ruterana, M. Morales, F. Gourbilleau, M. Wojdak, J. F. Carlin, M. Ilegems, and D. Chateigner, Superlattices Microstruct. **36**, 537 (2004).
[17] K. M. Yu, Z. Lilienthal-Weber, W. Walukiewicz, W. Shan, J. W. Ager, III, S. X. Li, R. E. Jones, E. E. Haller, H. Lu, and W. J. Schaff, Appl. Phys. Lett. **86**, 071910 (2005).
[18] P. Ruterana, P. Singh, M. Wojdak, J. L. Doualan, M. Morales, F. Gourbilleau, D. Massimo, W. Richter, and T. Schmidtling, Phys. Status Solidi A **202**, 781 (2005).